



HAL
open science

Macrophage plasticity is Rac signalling and MMP9 dependant

Jana Travnickova, Sandra Nhim, Naoill Abdellaoui, Farida Djouad, Mai Nguyen-Chi, Andrea Parmeggiani, Karima Kissa

► **To cite this version:**

Jana Travnickova, Sandra Nhim, Naoill Abdellaoui, Farida Djouad, Mai Nguyen-Chi, et al..
Macrophage plasticity is Rac signalling and MMP9 dependant. 2019. hal-02106150

HAL Id: hal-02106150

<https://hal.science/hal-02106150v1>

Preprint submitted on 16 Dec 2020

HAL is a multi-disciplinary open access archive for the deposit and dissemination of scientific research documents, whether they are published or not. The documents may come from teaching and research institutions in France or abroad, or from public or private research centers.

L'archive ouverte pluridisciplinaire **HAL**, est destinée au dépôt et à la diffusion de documents scientifiques de niveau recherche, publiés ou non, émanant des établissements d'enseignement et de recherche français ou étrangers, des laboratoires publics ou privés.

1 **Macrophage plasticity is Rac signalling and MMP9 dependant.**

2 Jana Travnickova¹, Sandra Nhim¹, Naoill Abdellaoui¹, Farida Djouad², Mai Nguyen-Chi¹, Andrea
3 Parmeggiani^{1,3} and Karima Kissa^{1,*}.

4

5

6 ¹ LIPH, CNRS, INSERM, Univ Montpellier, Montpellier, France

7 ² Inserm U 1183, IRMB, F-34295, Montpellier, France

8 ³ Laboratoire Charles Coulomb, CNRS, Univ Montpellier, Montpellier, France

9

10 *Correspondence: karima.kissa-marin@umontpellier.fr

11

12

13

14 **26 402 characters including spaces**

15 **Abstract**

16 *In vitro*, depending on extracellular matrix (ECM) architecture, macrophages migrate
17 either in amoeboid or mesenchymal mode; while the first is a general trait of leukocytes, the latter
18 is associated with tissue remodelling via Matrix Metalloproteinases (MMPs). To assess whether
19 these stereotyped migrations could be also observed in a physiological context, we used the
20 zebrafish embryo and monitored macrophage morphology, behaviour and capacity to
21 mobilisation haematopoietic stem/progenitor cells (HSPCs), as a final functional readout.
22 Morphometric analysis identified 4 different cell shapes. Live imaging revealed that macrophages
23 successively adopt all four shapes as they migrate through ECM. Treatment with inhibitors of
24 MMPs or Rac GTPase to abolish mesenchymal migration, suppresses both ECM degradation and
25 HSPC mobilisation while differently affecting macrophage behaviour. This study depicts real
26 time macrophage behaviour in a physiological context and reveals extreme reactivity of these
27 cells constantly adapting and switching migratory shapes to achieve HSPCs proper mobilisation.

28

29 **Introduction**

30 Macrophages were for the first time identified as phagocytic cells responsible for pathogen
31 elimination (Metchnikoff, 1892). Over the past century, they were associated with homeostasis,
32 innate and adaptive immune responses, inflammation, tissue remodelling and cytokine production
33 (Gordon and Taylor, 2005; Wynn et al., 2013). Macrophages are the most plastic haematopoietic
34 cells present in all tissues; their diversity depends upon their location, their morphology, their
35 membrane receptors or surface markers (Wynn et al., 2013). Depending on tissue composition
36 they infiltrate and environmental constraints, macrophages adopt different migration modes
37 (Vérollet et al., 2011). In the course of a three-dimensional (3D) migration, macrophages can
38 either adopt an amoeboid or a mesenchymal migratory mode. In case of an amoeboid migration,
39 cells take on a round or polarised shape and migrate through the extracellular matrix (ECM).
40 Such a migration is Rho/Rock GTPases dependent. During mesenchymal migration,
41 macrophages degrade the ECM through proteinases secretions (e.g. Matrix Metalloproteinases or
42 MMPs) and cells take on an elongated shape. This second migratory mode is Rac GTPase
43 signalling dependent (Sanz-Moreno and Marshall, 2010; Vérollet et al., 2011).

44 In mouse and human, macrophage characterization was mainly performed *in vitro* using bone
45 marrow derived macrophages. Recently, the zebrafish model was used to resolve specific issues
46 during the developmental process or to address accurate pathologies. The transparency of
47 zebrafish embryos enables the live imaging and real time tracking of cell populations. We and
48 other groups have shown that two main waves of macrophages emerge from primitive and
49 definitive haematopoiesis during the zebrafish development (Gering and Patient, 2005; Herbomel
50 et al., 1999; Murayama et al., 2006). The initial wave takes place between 18 and 25 hours post
51 fertilization (hpf) in the yolk sac (Herbomel et al., 1999). The second wave occurs between 30
52 and 55 hpf in the aorta-gonad-mesonephros (AGM) (Gering and Patient, 2005; Murayama et al.,

53 2006) and generates the haematopoietic stem/progenitor cells (HSPCs) (Bertrand et al., 2010;
54 Kissa and Herbomel, 2010) which later will differentiate into all blood cells including
55 macrophages. Finally, a transient hematopoietic wave is initiated in the posterior blood island,
56 giving rise to the multilineage progenitor cells and erythromyeloid progenitors, which develop
57 into both erythroid and myeloid cells (Bertrand et al., 2007).

58 Recently, we demonstrated *in vivo* that primitive macrophages are crucial in the establishment of
59 a definitive haematopoiesis (Travnickova et al., 2015). Macrophages that accumulated in the
60 AGM degrade the ECM located in the vicinity of HSPCs via matrix metalloproteinase 9 (MMP-9)
61 secretions, thereby enabling them to migrate, enter the blood stream and colonise haematopoietic
62 organs.

63 In the present study, we provide an extensive analysis of macrophages in zebrafish embryos.
64 Using morphological analysis we were able to distinguish for the first time different macrophage
65 subtypes *in vivo*. By combining morphological analysis with live imaging we succeeded in
66 visualizing the dynamic behavioural patterns of individual macrophages during their migration
67 through the ECM.

68

69

70 **Results**

71 **Macrophage shape heterogeneity in the zebrafish embryo**

72 During the establishment of the definitive haematopoiesis, macrophages accumulated in the
73 AGM between 30 and 60 hpf degrade the ECM surrounding HSPCs via Mmp-9 secretions which
74 result in the mobilization of HSPCs (Travnickova et al., 2015). Using this physiological model,
75 we analysed the shape and behaviour of proteolytic macrophage in order to establish a potential
76 correlation. We first described the position and shape of macrophages in the AGM using the
77 *kdrl:eGFP//mpeg1:mCherry-F* double transgenic lines where the GFP protein highlighted vessels
78 and mCherry-F macrophage membranes (**Fig. 1A-B**). Figure 1A provides a schematic view of the
79 vessel and macrophage position as shown in Figure 1B. Using a 3D view (**Fig. 1B**) we were able
80 to determine the position of macrophages (white arrows) in the outer layer of the vein wall
81 between the vein and the aorta floor with different morphologies. The particle analysis of
82 macrophages from a maximum projected confocal acquisitions enabled us to distinguish and
83 quantify the various macrophage shapes. Three main morphological criteria were identified:
84 circularity, roundness and elongation factor (**Fig. 1C and Suppl. Table 1**). They revealed the
85 existence of 4 main shapes whose images are shown in **Figure 1D**. We named these 4 subgroups
86 - round (1), amoeboid (2), star-like (3) and elongated shape (4). While the round and elongated
87 shapes had already been described *in vitro*, the two remaining shapes might represent either
88 subgroups present *in vivo* or intermediate stages between round and elongated shapes. The main
89 difference between the amoeboid and star-like shapes lied in the presence in the amoeboid shape
90 of a main axis, i.e. polarity. The quantification of each shape revealed that amoeboid, star-like
91 and elongated shapes were equally present whereas the round shape remained sparse (**Fig. 1E**).

92

93 **Dynamics of macrophage migration *in vivo***

94 The analysis of macrophage shapes revealed the existence of four morphological subgroups
95 distributed in the zebrafish AGM. To assess the behaviour of each macrophage subgroup, we
96 imaged *Tg(Mpeg1:mCherry)* embryos over the course of one hour (acquisition every minute;
97 **Video 1**). We selected time frames in colour depth projection that illustrated the dynamics of
98 macrophages able to adopt different shapes within fifteen minutes (**Fig. 2A-F and Video 1**,
99 colour code scale). The outlines represent the shape of macrophages in the imaged area at the 9th
100 minute and enable us to draw a direct comparison with following time points. The colour depth
101 projection of confocal imaging enabled us to determine the depth of macrophage positions *in vivo*
102 and to demonstrate their ability to migrate in 3D patterns (**Video 1**). *In vivo* tracking of all
103 macrophages within a 60 minute timeframe demonstrated that no specific directionality was
104 maintained during their migration (**Fig. 2G**, n=23) as opposed to macrophages attracted to a
105 wound site as an example of typical oriented migration (**Fig. 2H**, n=27). The speed of migration
106 remained the same in both cases (data not shown). Subsequently, we quantified the evolution of
107 macrophage shapes over time. Every single macrophage in the AGM reveals an ability to change
108 shape within a very short time span (measured every 5 minutes) and to pass repeatedly through
109 distinct shape subgroups over a 30 minutes course (**Fig. 2I**, n=10). The round shape appeared less
110 frequently than others and live imaging showed that cells often adopted a round shape under two
111 specific conditions: during cell division or once the macrophage entered the bloodstream.

112 In conclusion, macrophage real time imaging completes the characterisation of mesenchymal
113 migrating macrophages and shows for the first time that they can adopt successive morphologies
114 for their migration in the 3D matrix.

115

116

117 **Rac inhibition modifies macrophage behaviour and function**

118 Using *in vivo* imaging we showed that macrophages exhibited morphological plasticity during
119 their migration. This high plasticity depended on both, external (the stroma rigidity) and intrinsic
120 parameters (cytoskeleton dynamics) (Vérollet et al., 2011). One intrinsic factor associated with
121 mesenchymal migration is the small GTPase- Rac signalling. We thus investigated the effect of
122 Rac chemical inhibition on macrophage shape and migration patterns. The macrophage shape
123 distribution in Rac inhibitor (NSC23766) treated embryos did not significantly differ from that of
124 DMSO treated control (**Fig. 3A**, $N_{\text{DMSO}}=10$ and $N_{\text{Rac inh.}}=15$ embryos). Selected images from
125 **Video 2** (colour, depth, projection, bottom) demonstrated that the macrophage migration was
126 much slower than that of control embryos (**Fig. 3B-E, Video 2**, top). Macrophage speed
127 measured over 60 minutes in the AGM confirmed a decrease in velocity from 2.37 ± 0.13
128 $\mu\text{m}\cdot\text{min}^{-1}$ to $1.13 \pm 0.16 \mu\text{m}\cdot\text{min}^{-1}$ (**Fig. 3F**).

129 The tracking plot diagram illustrated macrophage migration path and distance in control and Rac-
130 inhibited embryos (**Fig. 3G-H**, $n=15$ macrophages from 4 embryos, position measured every
131 minute over 1 hour) and revealed that Rac inhibition reduced macrophage moves from 130.9 ± 7.5
132 μm to $56.8 \pm 7.8 \mu\text{m}$. Moreover, the analysis of macrophage shape dynamics, revealed a
133 reduction in macrophage plasticity over time as macrophages were no longer able to
134 consecutively adopt different shapes (**Fig. 3I, right**; $n= 7$) versus control (**Fig. 3I, left**; $n= 7$).
135 However, in spite of reduced plasticity levels, membrane extensions were still formed at the same
136 rate and with similar length as in control macrophages. Rac inhibition resulted in an increase in
137 single extension span (from 2.8 ± 0.3 min to 11.0 ± 1.9 min, $n_{\text{extension}}= 45$) as opposed to that of
138 control macrophages.

139 As macrophage migration and morphological plasticity were significantly affected by Rac
140 inhibition, we decided to evaluate the functionality of these macrophages. The main role of AGM

141 macrophages is to degrade the ECM and to enable HSPC migration (Travnickova et al., 2015). *In*
142 *vivo* zymography of *Tg(Mpeg1:mCherry)* embryos at 48 hpf, revealed a significant reduction in
143 gelatin degradation and thereby a lower gelatinase activity (decreased number of green dots of
144 cleavage-revealed FITC) in Rac inhibited embryo compared to control (**Fig. 3J**). Since the
145 proteolytic function of macrophages in the AGM is essential to HSPC mobilisation, we assessed
146 the effect of Rac inhibition on haematopoietic organ colonisation. We noticed an increase in
147 HSPCs accumulated in the AGM at 48 hpf ($+70\pm 8\%$, $n=6$) and consequently a decrease in HSPC
148 accumulated in the CHT at 55 hpf ($-41\pm 2\%$; $n=5$).

149

150

151 **MMP inhibition affects macrophage shape, behaviour and function.**

152 Rac inhibition has an impact on macrophage proteolytic activity and consequently on their
153 function. To assess whether direct inhibition of macrophage proteolytic activity induces a similar
154 behaviour, we soaked embryos in a medium containing SB-3CT MMP inhibitor. We previously
155 demonstrated that ECM degradation occurred as a result of macrophage-secreted MMP-9 around
156 HSPCs to enable their intravasation. We evaluated the direct impact of MMP inhibition on
157 macrophage morphology and noticed a variation in shape distribution: an increase in round shape
158 number and a decrease in star-like and elongated shapes (**Fig. 4A**). Moreover, MMP inhibition
159 affected macrophage migration and behaviour (**Fig. 4B-E, Video 3**). Selected images from **Video**
160 **3** displayed a typical example of macrophage migration pattern. Using Colour depth projection
161 we were able to visualise the 3D migration of macrophages in the AGM and noticed that in
162 MMP-9 inhibited embryos, macrophages migrated mainly in 2D. At a given point in time, they
163 adopted a single colour whereas in control embryos we observed dynamic changes indicated by
164 the presence of several colours at one time point (**Fig. 2A-F**). Moreover, **Video 3** showed the

165 macrophages adopted different migration pattern resembling to the leukocyte crawling on vein
166 vessel.

167 Furthermore, we observed that MMP inhibition affected macrophage velocity and directionality.
168 The speed of migration increased more than 3 times compared to the control (from 2.20 ± 0.11
169 $\mu\text{m}\cdot\text{min}^{-1}$ to $7.80 \pm 0.92 \mu\text{m}\cdot\text{min}^{-1}$; **Fig. 4F**). Finally, a tracking plot diagram which illustrated the
170 migration path and distance of macrophages in the AGM in control and MMP-inhibited embryos
171 (**Fig. 4G and H**) revealed that migration directionality increased from 0.27 to 0.66. Cell tracking
172 showed that macrophages migrated along the vein, in the same direction as the blood flow. We
173 concluded that, MMP inhibition affected both macrophage shape and migration patterns. They
174 adopted a MMP independent migration pattern with increased velocity which was reminiscent of
175 an amoeboid type of migration.

176

177

178

179 **Discussion**

180 In this study we characterised in zebrafish embryos the macrophage population present in the
181 AGM with a known proteolytic function (Travnickova et al., 2015). We reported the existence of
182 four macrophage morphological subgroups. Previous studies performed *in vitro* described two
183 major morphological types, elongated and rounded shapes (McWhorter et al., 2013). Using *in*
184 *vivo* analyses we were able to identify two additional morphological shapes: amoeboid and star-
185 like shapes. *In vivo* observations revealed the presence of a higher number of macrophage
186 subgroups in contrast to conclusions drawn from assays on 3D matrices, thereby suggesting the
187 importance of *in vivo* modelling to complete results obtained *in vitro*. Using high resolution live
188 imaging in conjunction with macrophage shape descriptor analysis we devised a novel tool that
189 enabled to quantify *in vivo* the dynamics and morphological plasticity of macrophages.

190 While macrophages were thought to exclusively migrate using an amoeboid mode (Friedl and
191 Weigelin, 2008), Dr Parini's group demonstrated their capacity to also use a mesenchymal
192 migration mode (Cougoule et al., 2012). In line with this last study, we describe the mesenchymal
193 macrophage migration process *in vivo* in zebrafish embryos. Macrophages revealed an increase in
194 shape plasticity which confirmed the outcome of previous studies performed *in vitro* (Cougoule
195 et al., 2012).

196 Previous studies highlighted the significance of the role played by Rac signalling in cytoskeleton
197 organisation during the mesenchymal migration of cells (Sanz-Moreno and Marshall, 2010). Our
198 study performed *in vivo* during the establishment of haematopoiesis in zebrafish embryos also
199 demonstrated that the mesenchymal migration of macrophages was Rac signalling dependent.
200 Going further, we observed that Rac signalling inhibition affected not only macrophage migration
201 but also their proteolytic function and their phenotype. Indeed, upon Rac inhibition macrophages

202 lose their ability to degrade the ECM matrix. We also observed that this treatment significantly
203 reduced macrophage velocity and morphological plasticity. Moreover, live imaging revealed that
204 macrophages develop and keep longer membrane extensions and that they remained longer in a
205 specific location. Our study confirmed previous *in vitro* observations showing that *Rac1*^{-/-}
206 macrophages cultured on plastic exhibited additional membrane extensions when compared to
207 control macrophages (Wheeler et al., 2006).

208 We finally observed that the inhibition of the macrophage proteolytic function induces their
209 transition into a different type of migration mode corresponding to the adaptation of macrophages
210 to their new environment. They adopted a round shape with an amoeboid migration.
211 Macrophages were no longer able to migrate within the AGM stroma and they moved along the
212 vein wall.

213 Proteolytic macrophages in the AGM exhibited a high functional similarity to macrophages
214 found in solid tumours referred to as tumour associated macrophages (TAM). TAM play a
215 significant part in ECM remodelling through proteinase releases (mainly MMP-2 and 9) and
216 allow tumour cells to join the bloodstream and to seed in secondary sites (Condeelis and Pollard,
217 2006). Therefore, a current strategy is to target TAM to combat cancer (Panni et al., 2013).
218 Several approaches based on macrophage depletion (clodronate liposomes) or functional
219 modification (broad spectrum MMP inhibitors) did not succeed and failed during clinical trials
220 due to low specificity and the amount of side effects (Panni et al., 2013; Turk, 2006). Expanding
221 our knowledge from a purely molecular standpoint toward an in-depth understanding of
222 behaviour and requirements in migration and site infiltration using adapted *in vivo* models, would
223 complement existing studies and enable us to develop more targeted immunotherapeutic solutions.

224

225 **Materials and Methods**

226 **Zebrafish husbandry**

227 Wild-type and transgenic lines were maintained in compliance with the Institutional Animal Care
228 and Use protocols. The following transgenic lines were used in this study: *Tg(Mpeg1:mCherry-F)*
229 (Ellett et al., 2011; Travnickova et al., 2015) for macrophage membrane marking and
230 *Tg(kdrl:eGFP)* (Beis et al., 2005) for vessel endothelium labelling. Embryos were kept in the
231 presence of 1-phenyl-2-thiourea to prevent melanin pigmentation (Westerfield, 2000) and staged
232 as described by Kimmel et al (Kimmel et al., 1995). All experiments were performed in
233 accordance with the protocol CEEA-LR-13007 approved by the Animal Care and Use
234 Languedoc-Roussillon Committee.

235

236 **Live Imaging**

237 Zebrafish embryos (lateral views, rostral to the left) were embedded in 0.7% low melting agarose
238 and imaged using a Zeiss LSM510 confocal microscope through a 40x water immersion objective
239 with a 1024x256 pixel resolution at 28°C. All live imaging experiments were performed at 46-48
240 hpf and all time-lapse imaging occurred at an acquisition rate of one minute at a 1µm z-interval.
241 The acquisitions were performed using ZEN2009. Image processing such as maximum intensity
242 projections, 3D view, and overall image contrast adjustment were performed using Fiji software.

243

244 **Inhibitor treatment**

245 Embryos were soaked in MMP-2 and 9 inhibitors SB-3CT (Enzo Life Sciences) 9 µM or
246 NSC23766 Rac inhibitor (Tocris) 50 µM or DMSO 0.25% as a control from 5-prim stage (25 hpf)
247 to 46-48 hpf. For stock solution, inhibitors were dissolved in DMSO at a 10mM concentration

248 and stored at -20°C .

249

250 **Image processing and macrophage shape analysis**

251 Confocal stacks of membrane-labelled macrophages were projected using a maximum intensity
252 projection and 2D images were binarised using an automatic threshold. The following shape
253 descriptors were evaluated using the Fiji plugin Particle analysis: area (μm^2), perimeter (μm),
254 circularity and roundness. The elongation factor was manually measured by dividing the longest
255 axis of the object by its longest perpendicular axis (x/y). Objects with an area under $80 \mu\text{m}^2$ were
256 excluded from the further analysis. Circularity was calculated using the following formula: $4\pi \times$
257 $(\text{area}/\text{perimeter}^2)$. This parameter varied from 0 (linear polygon) to 1 (perfect circle). Circularity
258 was used to set apart round objects (circularity > 0.2) and roundness and elongation factor
259 enabled us to break down non-round subjects into 3 subgroups: elongated, amoeboid and star-like
260 shaped. Roundness was calculated using the following formula: $4 \times \{\text{area}/ [\pi \times (\text{major axis})^2]\}$
261 and varied from 0 (linear polygon) to 1 (perfect round). Supplementary table 1 shows the mean
262 values of circularity, roundness and elongation factor measured for each of the above listed
263 subgroups.

264

265 **Cell tracking and velocity measurement**

266 Maximum intensity projections of 60 minute time-lapses acquired every minute were analysed
267 using a manual tracking plugin in Fiji. Measured data were transferred into a Chemotaxis and
268 Migration tool programme (Ibidi) to design tracking and rose plots (Figure 2G-H for rose plots,
269 3G-H and 4G-H for tracking plots). A rose diagram maps single counts of the position of every
270 macrophage in a selected area (black and grey sectors of angle $\pi/18$) every minute over 60
271 minutes with an $(x,y 0,0)$ starting point. The tracking plot diagram represents the migration path

272 and distance of macrophages in the AGM with an x,y 0,0 starting point, being measured every
273 minute over 60 minutes. The average of single macrophage velocities ($\mu\text{m min}^{-1}$) during 15-60
274 minutes were used for analysis. The evaluation of the directionality was performed using a
275 Rayleigh statistical test for the uniformity of a circular distribution of points (end points of single
276 macrophages). All analyses were conducted using the Chemotaxis and Migration tool software
277 (Ibidi).

278

279 **Fin amputation for oriented migration analysis**

280 Caudal fin amputation was performed with a sterile scalpel at 44 hpf, posterior to muscle and
281 notochord under anaesthesia with 0.016% Tricaine (ethyl 3-aminobenzoate, Sigma Aldrich). 4 h
282 post amputation embryos were mounted and imaged as described above.

283

284 ***In vivo* zymography**

285 The *In vivo* zymography was performed according to Crawford's protocol (Crawford and Pilgrim,
286 2005). A working solution, 1 mg ml^{-1} of fluoresceinated gelatin (Gelatin-FITC, Anaspec) in PBS
287 was injected (4-5 ng) into muscles between 4th and 5th somite at 42 hpf. Imaging was performed
288 following the injections. Embryos were incubated in DMSO or Rac inhibitor from 25 hpf up to
289 the Gelatin-FITC injections.

290

291 **Statistical analysis**

292 Normal distributions were analysed using the Shapiro-Wilk test. Non-Gaussian data were
293 analysed using the Wilcoxon test, Gaussian with Student t-test. $P < 0.05$ was considered as
294 statistically significant (symbols: **** $p < 0.0001$ *** $p < 0.001$; ** $p < 0.01$; * $p < 0.05$) Statistical
295 analyses were performed using the R software.

296

297 **Acknowledgements**

298 We would like to thank E. Lelièvre, M. Rossel and G. Lutfalla for their critical review of this
299 manuscript; V. Diakou and the MRI facility for their assistance, A. Sahuquet for his help in the
300 particle analysis. This work was supported by grants from the ARC, Chercheur d'Avenir -
301 Région Languedoc-Roussillon, FRM and ATIP-Avenir. J.T. was supported by a fellowship from
302 the MESR and FRM (FDT20150532507), M.N.-C. by a fellowship from the Université de
303 Montpellier.

304

305

306 **Author contributions**

307 J.T., and K.K. designed the project and the experiments, J.T., S.N., M.N.-C and N.A. performed
308 the experiments and analysed the results. J.T. and K.K. wrote the manuscript with the input of
309 S.N., M.N.-C. and F.D.

310

311 **Ethics**

312 All animal experiments described in the present study were conducted at the University of
313 Montpellier in compliance with European Union guidelines for handling of laboratory animals
314 (http://ec.europa.eu/environment/chemicals/lab_animals/home_en.htm) and were approved by the
315 Direction Sanitaire et Vétérinaire de l'Hérault and Comité d'Ethique pour l'Experimentation
316 Animale under reference CEEA-LR-13007.

317

318 **Disclosure of Conflicts of Interest**

319 The authors declare no competing financial interests.

320

321 **Abbreviations**

322 AGM, Aorta-Gonad-Mesonephros

323 HSPC, Haematopoietic stem and progenitor cells

324 MMP, Matrix metalloproteinases

325 TAM, Tumour associated macrophages

326 **References**

- 327 Beis, D., Bartman, T., Jin, S.-W., Scott, I.C., D'Amico, L. a, Ober, E. a, Verkade, H., Frantsve, J.,
328 Field, H. a, Wehman, A., et al. (2005). Genetic and cellular analyses of zebrafish atrioventricular
329 cushion and valve development. *Development* *132*, 4193–4204.
- 330 Bertrand, J.Y., Kim, A.D., Violette, E.P., Stachura, D.L., Cisson, J.L., and Traver, D. (2007).
331 Definitive hematopoiesis initiates through a committed erythromyeloid progenitor in the
332 zebrafish embryo. *Development* *134*, 4147–4156.
- 333 Bertrand, J.Y., Chi, N.C., Santoso, B., Teng, S., Stainier, D.Y.R., and Traver, D. (2010).
334 Haematopoietic stem cells derive directly from aortic endothelium during development. *Nature*
335 *464*, 108–111.
- 336 Condeelis, J., and Pollard, J.W. (2006). Macrophages: obligate partners for tumor cell migration,
337 invasion, and metastasis. *Cell* *124*, 263–266.
- 338 Cougoule, C., Van Goethem, E., Le Cabec, V., Lafouresse, F., Dupré, L., Mehraj, V., Mège, J.-L.,
339 Lastrucci, C., and Maridonneau-Parini, I. (2012). Blood leukocytes and macrophages of various
340 phenotypes have distinct abilities to form podosomes and to migrate in 3D environments. *Eur. J.*
341 *Cell Biol.* *91*, 938–949.
- 342 Crawford, B.D., and Pilgrim, D.B. (2005). Ontogeny and regulation of matrix metalloproteinase
343 activity in the zebrafish embryo by in vitro and in vivo zymography. *Dev. Biol.* *286*, 405–414.
- 344 Ellett, F., Pase, L., Hayman, J.W., Andrianopoulos, A., and Lieschke, G.J. (2011). Mpeg1
345 Promoter Transgenes Direct Macrophage-Lineage Expression in Zebrafish. *Blood* *117*, e49–e56.
- 346 Friedl, P., and Weigelin, B. (2008). Interstitial leukocyte migration and immune function. *Nat.*
347 *Immunol.* *9*, 960–969.
- 348 Gering, M., and Patient, R. (2005). Hedgehog signaling is required for adult blood stem cell
349 formation in zebrafish embryos. *Dev. Cell* *8*, 389–400.
- 350 Gordon, S., and Taylor, P.R. (2005). Monocyte and macrophage heterogeneity. *Nat. Rev.*
351 *Immunol.* *5*, 953–964.
- 352 Herbomel, P., Thisse, B., and Thisse, C. (1999). Ontogeny and behaviour of early macrophages
353 in the zebrafish embryo. *Development* *126*, 3735–3745.
- 354 Kimmel, C.B., Ballard, W.W., Kimmel, S.R., Ullmann, B., and Schilling, T.F. (1995). Stages of
355 embryonic development of the zebrafish. *Dev. Dyn.* *203*, 253–310.
- 356 Kissa, K., and Herbomel, P. (2010). Blood stem cells emerge from aortic endothelium by a novel
357 type of cell transition. *Nature* *464*, 112–115.
- 358 McWhorter, F.Y., Wang, T., Nguyen, P., Chung, T., and Liu, W.F. (2013). Modulation of
359 macrophage phenotype by cell shape. *Proc. Natl. Acad. Sci. U. S. A.* *110*, 17253–17258.
- 360 Metchnikoff, É. (1892). *Leçons sur la pathologie comparée de l' inflammation : faites à l'*
361 *Institut Pasteur en avril et mai 1891 / par Élie Metchnikoff* (Paris: Librairie de l'académie de
362 médecine, 120, Boulevard Saint-Germain, Paris).
- 363 Murayama, E., Kissa, K., Zapata, A., Mordelet, E., Briolat, V., Lin, H.-F., Handin, R.I., and

- 364 Herbolmel, P. (2006). Tracing hematopoietic precursor migration to successive hematopoietic
365 organs during zebrafish development. *Immunity* 25, 963–975.
- 366 Panni, R.Z., Linehan, D.C., and DeNardo, D.G. (2013). Targeting tumor-infiltrating macrophages
367 to combat cancer. *Immunotherapy* 5, 1075–1087.
- 368 Sanz-Moreno, V., and Marshall, C.J. (2010). The plasticity of cytoskeletal dynamics underlying
369 neoplastic cell migration. *Curr. Opin. Cell Biol.* 22, 690–696.
- 370 Travnickova, J., Tran Chau, V., Julien, E., Mateos-Langerak, J., Gonzalez, C., Lelièvre, E.,
371 Lutfalla, G., Taviani, M., and Kissa, K. (2015). Primitive macrophages control HSPC
372 mobilization and definitive haematopoiesis. *Nat. Commun.* 6, 6227.
- 373 Turk, B. (2006). Targeting proteases: successes, failures and future prospects. *Nat. Rev. Drug*
374 *Discov.* 5, 785–799.
- 375 Vérollet, C., Charrière, G.M., Labrousse, A., Cougoule, C., Le Cabec, V., and Maridonneau-
376 Parini, I. (2011). Extracellular proteolysis in macrophage migration: losing grip for a
377 breakthrough. *Eur. J. Immunol.* 41, 2805–2813.
- 378 Westerfield, M. (2000). *The Zebrafish book. A guide for the laboratory use of zebrafish (Danio*
379 *rerio)*, 4th edition (Eugene).
- 380 Wheeler, A.P., Wells, C.M., Smith, S.D., Vega, F.M., Henderson, R.B., Tybulewicz, V.L., and
381 Ridley, A.J. (2006). Rac1 and Rac2 regulate macrophage morphology but are not essential for
382 migration. *J. Cell Sci.* 119, 2749–2757.
- 383 Wynn, T. a, Chawla, A., and Pollard, J.W. (2013). Macrophage biology in development,
384 homeostasis and disease. *Nature* 496, 445–455.
- 385
- 386

387 **Figure Legends**

388 **Figure 1:** Macrophages in the AGM can be divided into 4 morphological subgroups.

389 (A) The drawing shows a 3D view of vessels and macrophages (red) imaged in B. (B) 3D view of
390 the AGM in the mid-trunk region of a *Tg(kdrl:eGFP//mpeg1:mCherry-F)* zebrafish embryo at 48
391 hpf showing the position of vessels (endothelium in green) and macrophages (in red, white
392 arrows) in the outer side of the vein and in between the dorsal aorta and the cardinal vein. (C)
393 Diagram of the 4 categories of macrophages delineated according to shape attributes– circularity,
394 roundness and elongation factor. (D) Representative confocal images (maximum intensity
395 projections) of individual categories with an outline drawing from particle analysis on the right.
396 (E) Graph representing the percentage distribution of the different shape categories per AGM.
397 Data are represented as percentage average \pm s.e.m. N= 20 embryos. C, caudal; D, dorsal; DA,
398 dorsal aorta; PCV, posterior cardinal vein; R, rostral; V, ventral. See also supplementary table 1.

399

400 **Figure 2:** Macrophages in the AGM migrate in the mesenchymal way and undergo dynamic
401 transition between different shapes over time.

402 (A-F) Selected images from Video 1 illustrate the macrophage migration and shape
403 transformation over time. Numbers point to individual macrophages. Time code is expressed in
404 hours and minutes. White outlines on panel B-F indicate the shape and position of macrophages
405 from panel A (9th minute). (G-H) Rose plot diagrams show the directionality of macrophage
406 migration in the AGM compared to the oriented migration of macrophages in the tail region after
407 tail fin cut injury. A diagram represents the single counts of the position of each macrophage in
408 the selected area (black and grey sectors of angle $\pi/18$) every minute over 60 minutes with a (x,y
409 0,0) starting point. n= 23 macrophages for the control and n=27 for directed migration. (I) Graph

410 showing the shape evolution of individual macrophages during a 30 minutes course with 5
411 minutes interval measurements. Every line represents a single macrophage (n= 10). See also
412 Video 1. Scale bar, (A-F) 30 μ m.

413

414 **Figure 3:** Rac inhibition leads to a loss of macrophage plasticity and motility.

415 (A) Graph comparing macrophage shape distribution in the AGM of NSC23766 Rac-inhibited
416 embryos (Rac Inh) to DMSO treated embryos (control) shows no significant change of
417 distribution. N=10 embryos for control and 15 for Rac inh. Data are represented as the mean of
418 the percentage of each shape type in the total macrophage population in the AGM \pm s.e.m. NS =
419 not significant. (B-E) Selected cropped images from Video 2 showing the shape and migration of
420 macrophages over time. Time code in hours and minutes. White outlines on panel C-E indicate
421 the shape and position of macrophages from panel B (21st minute) (F) Graph showing the
422 velocity of macrophages in control and Rac-inhibited embryos. Data are represented as a mean \pm
423 s.e.m., n= 15 macrophages from 4 different embryos, ****p<0.0001. (G-H) Tracking plot
424 diagram representing the migration path and distance of macrophages in the AGM in control and
425 Rac-inhibited embryos measured every minute for 60 minutes. Scale in μ m, n=15 macrophages
426 from 4 different embryos. (I) Graph shows the shape evolution of individual macrophages during
427 a 30 minute course with 5 minutes interval measurements, Control to the left, Rac inhibitor to the
428 right. Each line represents a single macrophage (n= 7). Statistically significant differences exist in
429 the number of shapes adopted during a 30 minute measurement course (P=0.003) as well as in the
430 number of changes between two different shapes (P=0.006). (J) *In vivo* zymography in
431 *Tg(Mpeg1:mCherry)* embryos at 48 hpf reveals the degradation of inserted gelatin (green dots of
432 cleavage-revealed FITC) in control embryos and a highly reduced degradation after Rac
433 inhibition. See also Video 2. Scale bar: 30 μ m.

434

435 **Figure 4:** MMP-9 inhibition induces a change in macrophage shape and a transition towards an
436 amoeboid-like migration.

437 (A) Graph compares the macrophage shape distribution in the AGM of MMP-2 and 9 (SB-3CT) -
438 inhibited embryos (MMP inh) to DMSO treated embryos (control) shows an increase in round
439 shape and a decrease in star-like and elongated shapes in MMP inh embryos. N=10 embryos for
440 control and 15 for MMP inh. Data represent the percentage mean for each shape type out of the
441 total number of macrophages in the AGM \pm s.e.m. NS = not significant; * $p < 0.05$; **** $p < 0.0001$.

442 (B-E) Selected cropped images from Video 3 displays macrophage shape and migration patterns
443 over time. Numbers point to individual macrophages, time code is expressed in hours and
444 minutes. Grey outlines on panel C-E show the shape and position of macrophages from panel B
445 (3rd minute). (F) Graph showing the velocity of macrophages in control and MMP-inhibited
446 embryos. Data are represented as a mean \pm s.e.m., n= 17 macrophages for control and 14 for
447 MMP inhibitor from 4 different embryos, **** $p < 0.0001$. (G-H) Tracking plot diagram represents
448 the migration path and distance of macrophages in the AGM in control and MMP-inhibited
449 embryos measured every minute over 60 minutes. Scale in μm , n=17 macrophages for control
450 and 14 for MMP inhibitor from 4 different embryos. See also Video 3. Scale bar 30 μm . DA,
451 dorsal aorta; PCV, posterior cardinal vein.

452

453 **Supplementary table 1:** Measured average values (\pm s.e.m.) of shape descriptors for each shape
454 subgroup. N = 20 embryos.

455

456 **Video 1:** Macrophage 3D migration in the AGM during haematopoiesis.

457 Representative time-lapse colour-depth projections of *Tg(mpeg1:mCherry)* embryo at 46 hpf

458 illustrate macrophages migration occurring in a non-directional manner and through different
459 depth by appropriately changing colour . Image stacks were acquired every minute over 60
460 minutes at a 1 μm interval with 1024x256 pixel resolution using the LSM510 Zeiss confocal
461 microscope equipped with a 40x water immersion objective. Scale bar 30 μm , time code in hours
462 and minutes.

463

464 **Video 2:** The migratory behaviour of macrophage changes after Rac inhibition.

465 Combined representative time-lapse colour-depth projections of *Tg(mpeg1:mCherry)* embryos at
466 46 hpf draws a comparison between macrophage migration in DMSO-treated (control, top)
467 embryos and that of Rac-inhibitor (Rac inh, bottom) treated embryos. Rac-inhibited macrophages
468 display slower migration modes. They change shapes and migration direction less often, and form
469 very long membrane extensions. Image stacks were acquired every minute over 60 minutes at a 1
470 μm interval with 1024x256 pixel resolution using the LSM510 Zeiss confocal microscope
471 equipped with a 40x water immersion objective. Scale bar 30 μm , time code in hours and minutes.

472

473 **Video 3:** MMP inhibition induces mesenchymal-amoeboid transition of macrophage migration.

474 Combined representative time-lapse colour-depth projections of *Tg(mpeg1:mCherry)* embryos at
475 46 hpf draw a comparison between macrophage migration in DMSO-treated (control, top) and
476 MMP-2 and 9 inhibitor (MMP inh, bottom) treated embryos. MMP-inhibited macrophages
477 migrate faster, adopt a round shape, change the depth of their displacement less often and migrate
478 partially inside the bloodstream. Image stacks were acquired every minute over 60 minutes at 1
479 μm interval with 1024x256 pixel resolution using the LSM510 Zeiss confocal microscope
480 equipped with a 40x water immersion objective. Scale bar 30 μm , time code expressed in hours
481 and minutes.

Figure 1

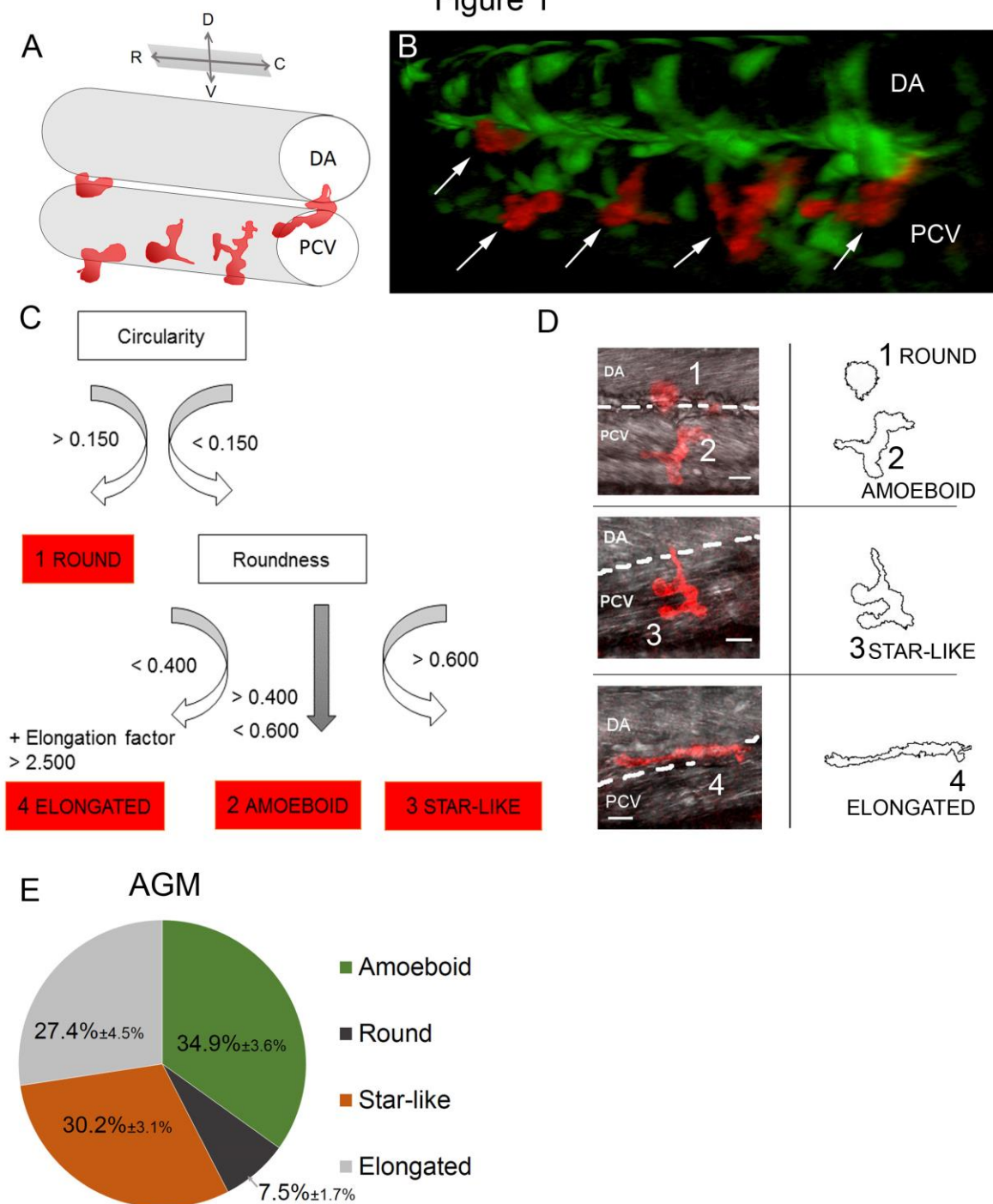


Figure 2

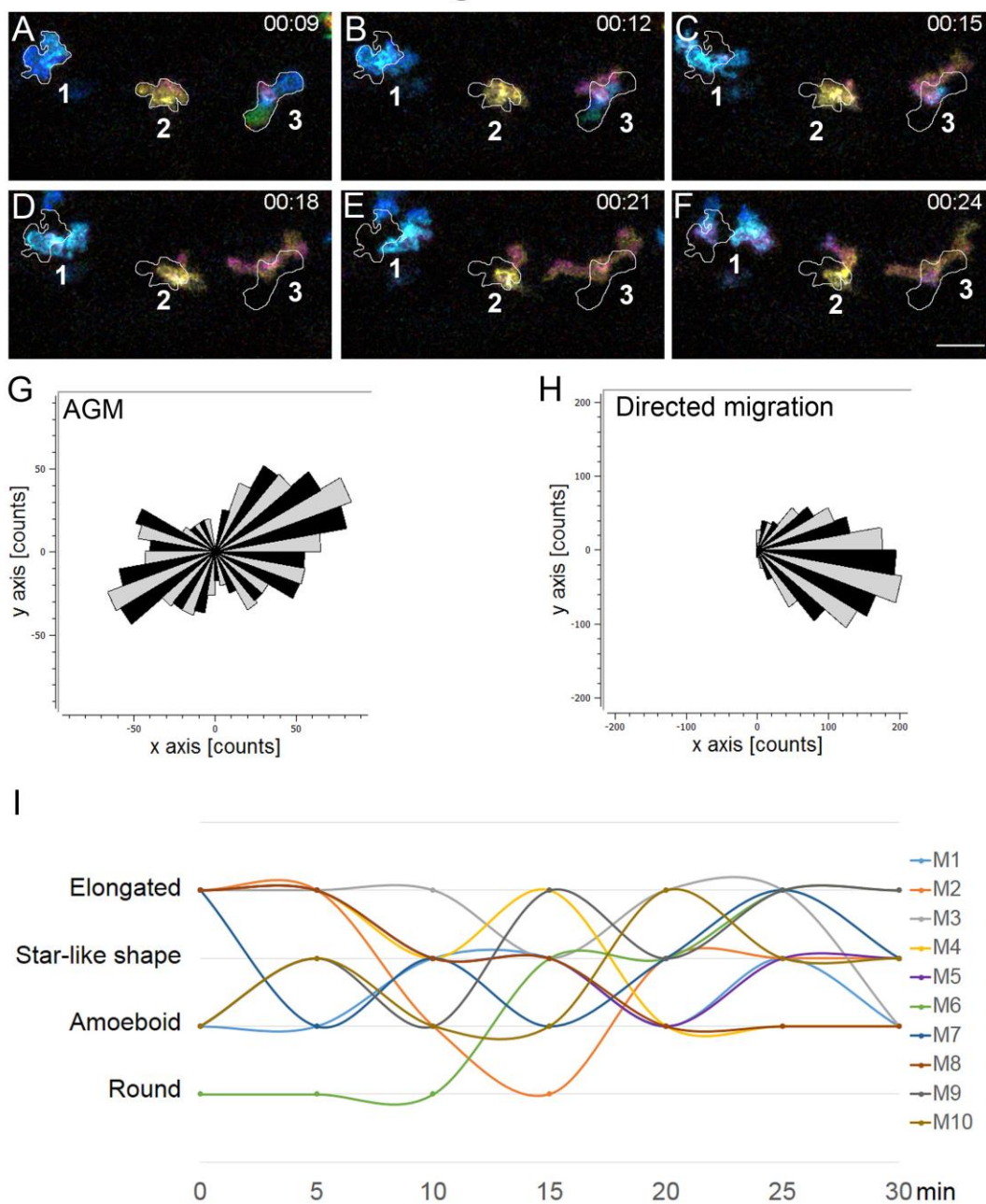


Figure 3

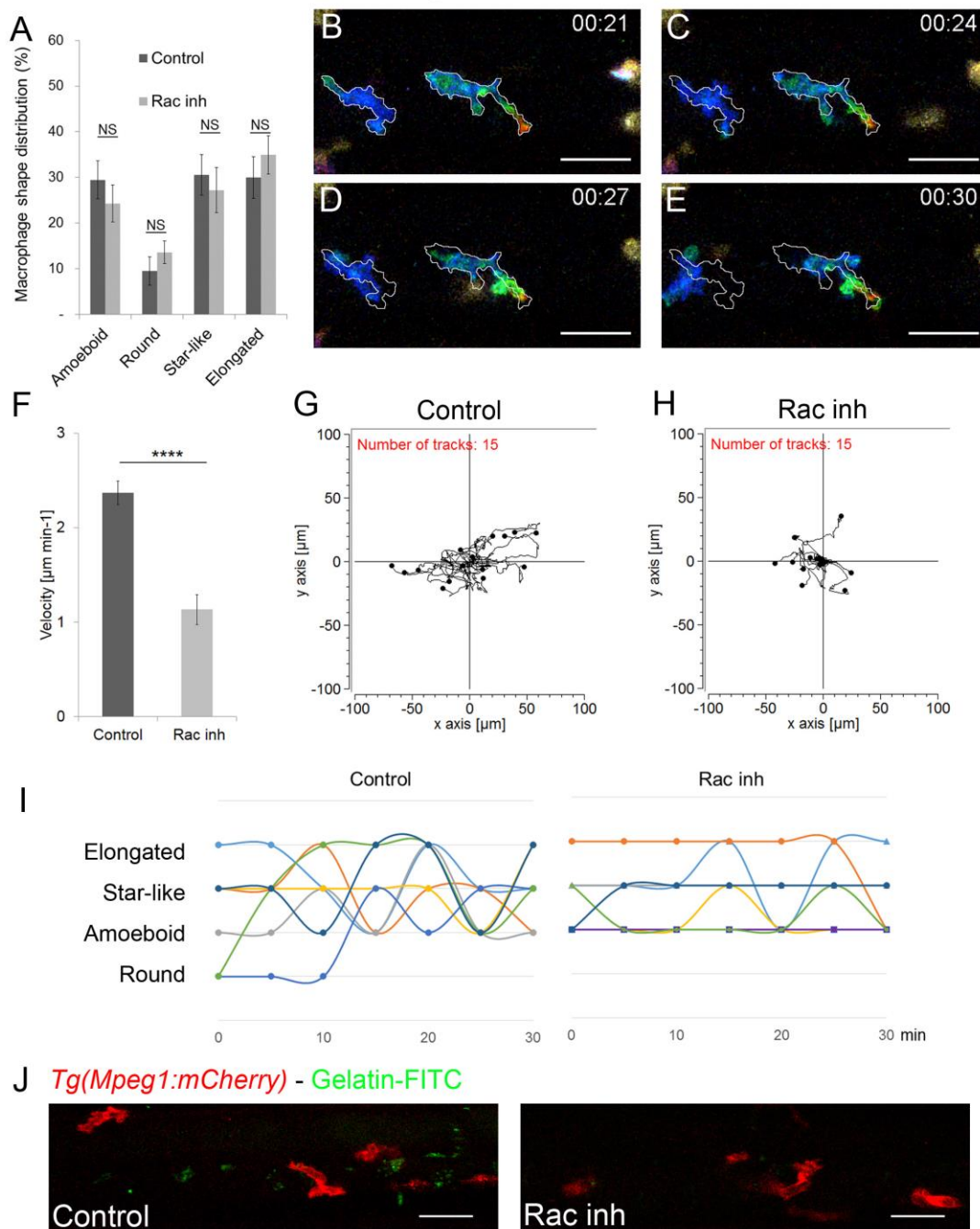
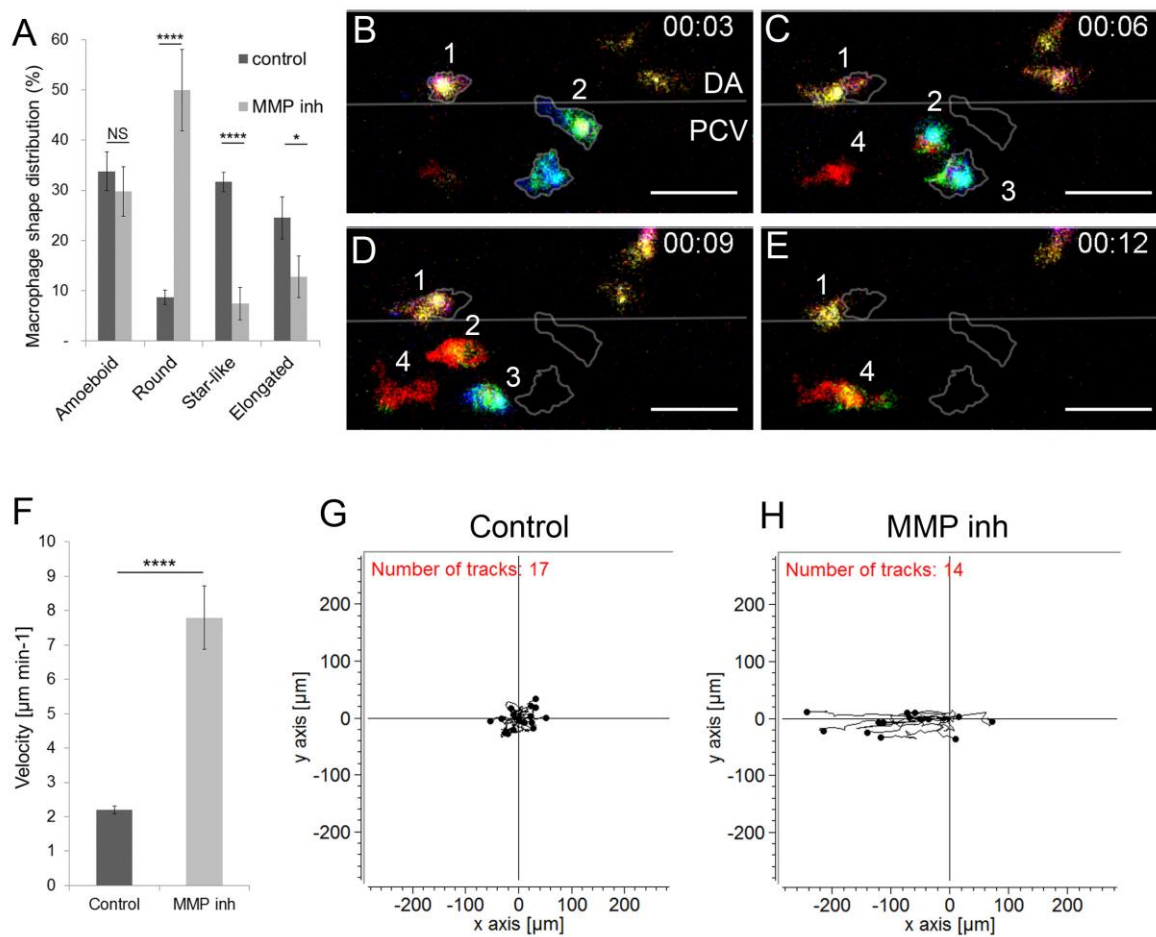


Figure 4



485

486

487 **Supplementary Table 1.**

488

Shape	Circularity	Roundness	Elongation factor
Round	0.19 ± 0.01	0.65 ± 0.04	1.55 ± 0.10
Amoeboid	0.07 ± 0.004	0.49 ± 0.01	2.04 ± 0.05
Star-like	0.07 ± 0.004	0.70 ± 0.01	1.56 ± 0.07
Elongated	0.07 ± 0.005	0.35 ± 0.01	3.45 ± 0.14

489